Layer-dependent topological phase in a two-dimensional quasicrystal and approximant

Jeffrey D. Cain[a,b,c,1], Amin Azizi[a,c,1], Matthias Conrad[d], Sinéad M. Griffin[b,e], and Alex Zettl[a,b,c,2]

[a]Department of Physics, University of California, Berkeley, CA 94720; [b]Materials Sciences Division, Lawrence Berkeley National Laboratory, Berkeley, CA 94720; [c]Kavli Energy NanoSciences Institute, University of California, Berkeley and Lawrence Berkeley National Laboratory, Berkeley, CA 94720; [d]Fachbereich Chemie, Philipps-Universität Marburg, 35032 Marburg, Germany; and [e]The Molecular Foundry, Lawrence Berkeley National Laboratory, Berkeley, CA 94720

Edited by Angel Rubio, Max Planck Institute for the Structure and Dynamics of Matter, Hamburg, Germany, and approved August 24, 2020 (received for review July 17, 2020)

The electronic and topological properties of materials are derived from the interplay between crystalline symmetry and dimensionality. Simultaneously introducing "forbidden" symmetries via quasiperiodic ordering with low dimensionality into a material system promises the emergence of new physical phenomena. Here, we isolate a two-dimensional (2D) chalcogenide quasicrystal and approximant, and investigate their electronic and topological properties. The 2D layers of the materials with a composition close to $Ta_{1.6}Te$, derived from a layered transition metal dichalcogenide, are isolated with standard exfoliation techniques, and investigated with electron diffraction and atomic resolution scanning transmission electron microscopy. Density functional theory calculations and symmetry analysis of the large unit cell crystalline approximant of the quasicrystal, $Ta_{21}Te_{13}$, reveal the presence of symmetry-protected nodal crossings in the quasicrystalline and approximant phases, whose presence is tunable by layer number. Our study provides a platform for the exploration of physics in quasicrystalline, low-dimensional materials and the interconnected nature of topology, dimensionality, and symmetry in electronic systems.

two-dimensional materials | quasicrystals | approximant | scanning transmission electron microscopy | topological materials

In recent decades, two discoveries have caused dramatic shifts in the descriptions of order in solid-state systems: the prediction and subsequent observation of topological order, and the discovery of Bragg diffraction in aperiodic quasicrystals. Topological phases are defined by geometric phases of the underlying wave function which result in unusual properties, like boundary states that are robust to disorder. Interest in topological matter has surged since the discoveries of an ever-expanding collection of materials with symmetry-protected features. Experimentally realized topological materials include topological (1–3) and Chern insulators and Dirac and Weyl semimetals (4–8).

A similar paradigm shift was brought about by the discovery of aperiodic order and so-called "forbidden" symmetries in quasicrystalline materials (9). Quasicrystals may occur when a structure has long-range order which is not compatible with long-range translational symmetry. This incompatibility can arise from the presence of specific symmetries (e.g., 5-, 8-, 10-, and 12-fold) which are not compatible with translational symmetry (unlike, for example, 4- or 6-fold symmetries). Examples of aperiodic tilings include, pentagonal, dodecagonal (dd), and Penrose tilings (10). First demonstrated in quenched aluminum alloys (9), quasicrystalline order has been observed in other metallic systems (11), self-assembled colloidal crystals (12), ultracold atoms (13), and chemical vapor deposition (CVD)-grown bilayer graphene (14–16).

Recent work has reexamined what classes of systems can host topological phenomena, and the catalog has expanded to include amorphous materials (17, 18) and light elements (19). Additionally, several theoretical works have examined the influence of aperiodicity and quasicrystallinity on topological phases (20) including pentagonal (21) and octagonal (22) quasicrystals and so-called "higher-order topological insulators" (23). Further, topological polarization not possible in periodic crystals has been theoretically proposed to exist in quasicrystals. Artificial quasiperiodic systems have been created experimentally in photonic crystals, wherein a photonic waveguide was used to construct a 1D Hamiltonian with 2D topological edge modes (24). The 2D quasicrystals have specifically been predicted to host novel electronic states, including Hofstadter's Butterfly (25) and the four-dimensional quantum Hall effect (26); however, to date, no specific quasicrystalline solid-state system has been proposed that can host nontrivial electronic topological states. There are examples of low-dimensional, quasicrystalline solids in the literature; specifically, CVD-grown 30° bilayer graphene (27) and 2D $BaTiO_3$ epitaxially grown on Pt (28). However, quasicrystallinity has not been observed in exfoliated materials, limiting the exploration of quasicrystalline order in 2D materials and van der Waals heterostructures.

In the binary tantalum–tellurium system, a layered-type quasicrystalline phase exhibiting a 12-fold symmetric diffraction pattern was discovered (29). The composition of this dd phase is close to $Ta_{1.6}Te$. In intimate proximity to dd-$Ta_{1.6}Te$ exist several crystalline phases, so-called approximants, that are compositionally and structurally closely related to the quasicrystalline compound.

Significance

The behavior of electrons in solids is intimately related to symmetry and dimensionality, and it is the interaction of these two that dictates the topological properties of materials. Here, we study this by introducing quasiperiodic order into a two-dimensional material, expanding the catalogue topological systems to include quasicrystals. Specifically, we report the isolation and investigation of a two-dimensional chalcogenide quasicrystal and approximant, ~$Ta_{1.6}Te$, derived from a layered transition metal dichalcogenide. Density functional theory of a large unit cell approximant demonstrates that the material possesses a layer-tunable, topologically nontrivial band structure, hitherto unseen in quasicrystalline materials. This work lays the foundation for the study of the interrelated properties of dimensionality, topology, and symmetry in van der Waals solids and heterostructures.

Author contributions: J.D.C. and A.Z. designed research; J.D.C., A.A., M.C., and S.M.G. performed research; J.D.C., A.A., M.C., S.M.G., and A.Z. analyzed data; and J.D.C., A.A., M.C., S.M.G., and A.Z. wrote the paper.

The authors declare no competing interest.

This article is a PNAS Direct Submission.

[1]J.D.C. and A.A. contributed equally to this work.

[2]To whom correspondence may be addressed. Email: azettl@berkeley.edu.

This article contains supporting information online at https://www.pnas.org/lookup/suppl/doi:10.1073/pnas.2015164117/-/DCSupplemental.

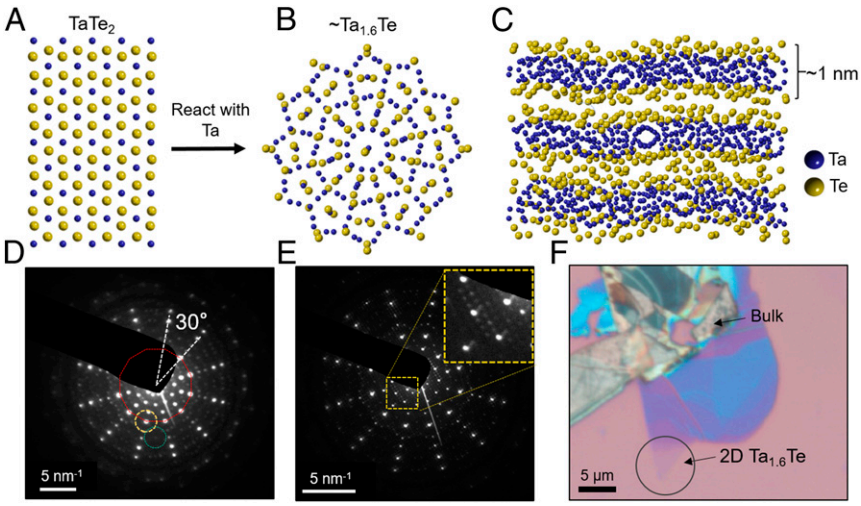

Fig. 1. Structure of 2D $Ta_{1.6}Te$. (*A*) $TaTe_2$ and (*B*) Ta–Te cluster within dd-$Ta_{1.6}Te$ and $Ta_{181}Te_{112}$ approximant. (*C*) Side view of the layered structure showing the Te–Ta–Te slabs, 1 nm thick. (*D*) Electron diffraction pattern of dd-$Ta_{1.6}Te$ showing 12-fold symmetry (red) and self-similar motifs (green and yellow). (*E*) Electron diffraction of the large unit cell approximant $Ta_{181}Te_{112}$. (*Inset*) Magnified area showing periodic superstructure. (*F*) Optical microscope image of exfoliated $Ta_{1.6}Te$, with 2D section highlighted within black circle.

The structures of two approximants, $Ta_{97}Te_{60}$ (30) and $Ta_{181}Te_{112}$ (31), were determined by means of single-crystal X-ray diffraction, whereas $Ta_{21}Te_{13}$ (31) was identified by means of electron diffraction and high-resolution electron microscopy. Based upon the knowledge of the structures of $Ta_{97}Te_{60}$ and $Ta_{181}Te_{112}$, the building principle underlying the approximant structures was deciphered. This building principle allows for the derivation of structure models of new approximants, as was shown for $Ta_{21}Te_{13}$. Furthermore, the algorithm can be used for generating structure models for the quasicrystalline phase.

Here, we expand the catalog of exfoliated 2D materials to include quasicrystals and approximants; specifically, the van der Waals material dd-$Ta_{1.6}Te$ (29) and $Ta_{181}Te_{112}$ approximant (31). We isolate a few layers of the materials and investigate their structure using electron diffraction and atomic resolution scanning transmission electron microscopy. Using first-principles calculations and symmetry analysis performed on the large unit cell crystalline approximant, $Ta_{21}Te_{13}$ (31), we calculate the material's electronic structure and find that it can host symmetry-protected nodal states, whose presence is dependent upon layer number.

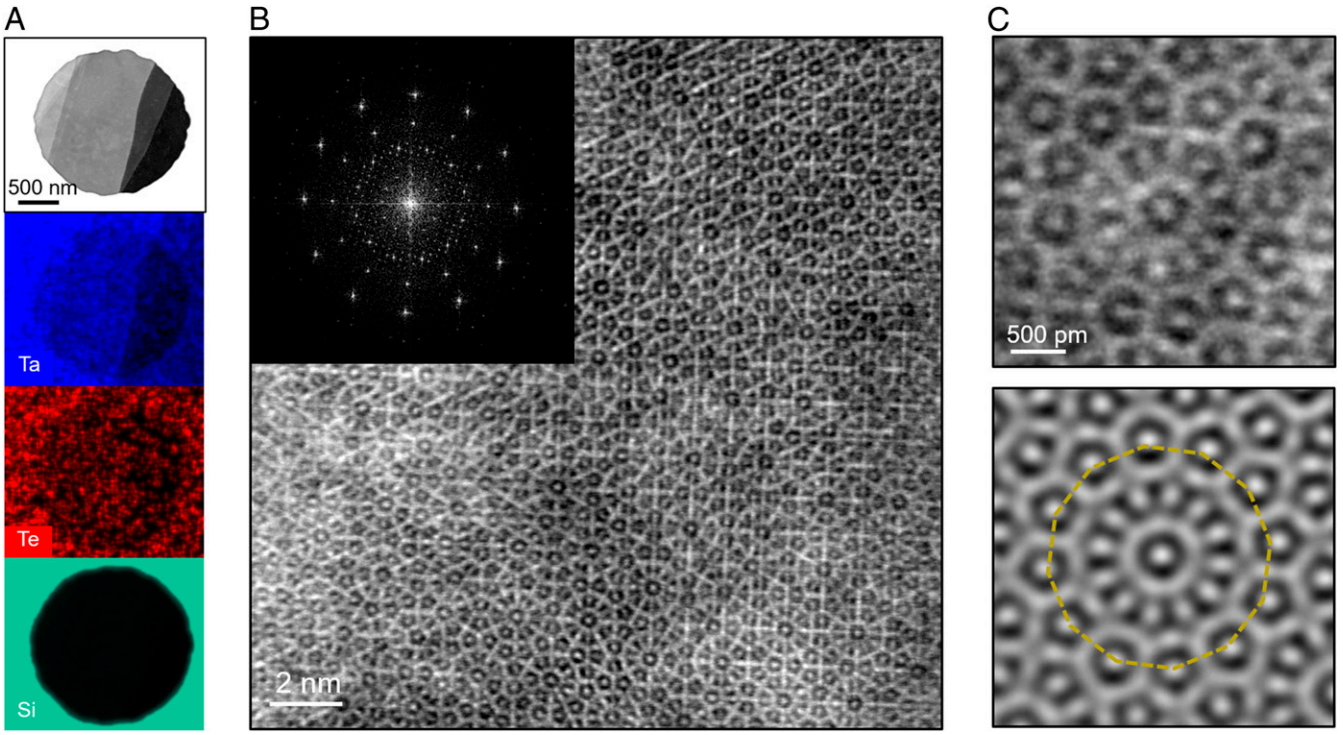

Fig. 2. High-resolution imaging of $Ta_{181}Te_{112}$. (*A*) EDS maps and reference image showing uniform distribution of Ta and Te in the material (see *SI Appendix*, Fig. S4 for the EDS spectrum). (*B*) Low-magnification STEM image. *Inset*: Fourier Transform of image. (*C*) High-magnification image of Ta–Te cluster, (*Top*) unfiltered and (*Bottom*) filtered.

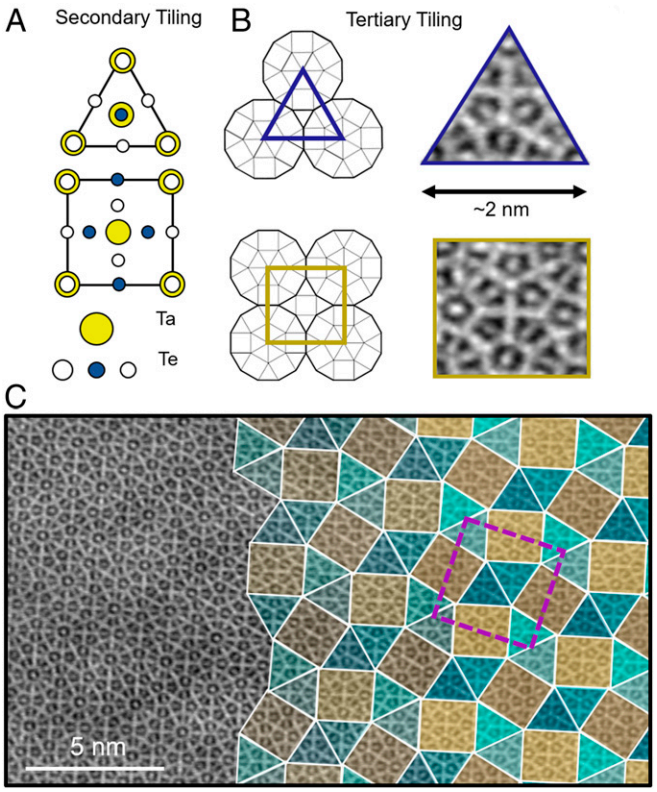

Fig. 3. Tiling of $Ta_{181}Te_{112}$. (*A*) Secondary tiling with atoms, and (*B*) tertiary triangle and square tiles used to tile the $Ta_{181}Te_{112}$ lattice. (*C*) Tiled image of $Ta_{181}Te_{112}$ (unit cell highlighted in purple).

The material is prepared by reducing the transition metal dichalcogenide $TaTe_2$ (32) at high temperature with Ta, as previously reported by one of the authors in Conrad et al. (29) (see *SI Appendix* for synthesis details). The resulting material appears to be a mixture of the dd phase and approximant ($Ta_{181}Te_{112}$). The processing induces a step-wise transformation from the monoclinic $TaTe_2$ structure (Fig. 1*A*) into the dd quasicrystalline form dd-$Ta_{1.6}Te$ and $Ta_{181}Te_{112}$. Common to the dd phase and approximants are 12-fold Ta–Te clusters, shown in Fig. 1*B*. Both compounds exhibit anisotropic structures, with out-of-plane (periodic) Te terminated layers, separated by a van der Waals gap, analogous to the transition metal dichalcogenides (e.g., MoS_2, WSe_2). For both the dd phase and approximant, the layers are ∼1 nm thick (Fig. 1*C*). The resulting crystals are hundreds of microns in diameter, and exhibit platelet-like morphology with a metallic gold luster and an obvious lamellar, lubricant-like structure. The resulting material is unstable in ambient atmosphere and is stored and handled in an inert atmosphere (see *SI Appendix* for details). Electron microscopy sample preparation details, along with optical images of the transferred material, are presented in *SI Appendix*, Fig. S1. Electron diffraction of the dd-$Ta_{1.6}Te$ is shown in Fig. 1*D*. The diffraction pattern exhibits 12-fold symmetric spots (red dodecagon), separated by 30°. The pattern also shows the self-similar, multiscale, 12-fold symmetric structure (green and yellow dodecagons) characteristic of quasicrystalline materials. An electron diffraction pattern from the approximant phase, $Ta_{181}Te_{112}$, is shown in Fig. 1*E*; the periodic superstructure is easily seen in Fig. 1 *E*, *Inset*, indicating the presence of periodicity and translational symmetry in the lattice. As noted above, the samples of the materials are lamellar, and easily cleaved with the "scotch tape" method. This is demonstrated by the optical image in Fig. 1*F* which shows that the materials can be exfoliated into their 2D building blocks. The 2D samples of $Ta_{1.6}Te$ are identified by optical contrast, and ultrathin samples are readily produced using standard exfoliation techniques (*SI Appendix*, Fig. S2). Further, *SI Appendix*, Fig. S3 shows a low-magnification annular dark-field scanning transmission electron microscope (ADF-STEM) image, which shows the discrete layers of the exfoliated material.

The structure of $Ta_{181}Te_{112}$ is next investigated using electron microscopy and atomic resolution STEM imaging. First, the composition is mapped in Fig. 2*A* using energy-dispersive X-ray spectroscopy (EDS), along with a reference image, which shows homogenous distribution of Ta and Te (see the EDS spectrum in *SI Appendix*, Fig. S4). Fig. 2*B* shows a low-magnification ADF-STEM image of the material, in which 12-fold Ta–Te clusters are evident. From the image, it is not immediately evident which phase is present; therefore, Fig. 2 *B*, *Inset* shows a Fourier transform of the image in which the periodic superstructure (square pattern of dots) of the approximant can be clearly seen. Further, high-magnification images of a Ta–Te cluster (Fig. 2 *C*, *Top*: unfiltered; Fig. 2 *C*, *Bottom*: filtered) are shown. The structures of dd-$Ta_{1.6}Te$ and its approximants can be characterized by square–triangle tilings on different length scales. The basic or secondary tiling consists of tiles with an edge length of about 0.5 nm, which are shown together with their decoration with Ta and Te atoms in Fig. 3*A*. These tiles are then combined into the dodecahedral motifs, yielding squares and triangles with an edge length of about 2 nm, presented in Fig. 3*B* (schematic and ADF-STEM images). These tiles span the so-called tertiary tiling. If this algorithm is repeated ad infinitum, we obtain a self-similar square–triangle tiling which was first described by Stampfli (33), and may be used as a model for the quasicrystalline phase. Note that the dodecahedral motifs can occur in two orientations which are related by a rotation of about 30°. The same tiles with 2-nm edge length are used to tile both the dd and approximant structures, with local atomic structure shared in both phases. Fig. 3*C* shows a partially tiled image of $Ta_{181}Te_{112}$; rather than tiling in an aperiodic fashion of the dd structure, a periodic tiling is achieved. The unit cell of the approximant is highlighted in purple. In this image, all of the triangle tiles have the same local atomic structure, and all of the square tiles have the same local atomic structure. Tiles with the same color have the same orientation within the image.

To investigate the electronic structure of the dd-$Ta_{1.6}Te$ quasicrystal and its approximant, as well as their evolution upon going from three dimensions to two, we consider another approximant material, $Ta_{21}Te_{13}$, so that we may apply density functional theory (DFT) methods to the system, which require Bloch periodicity. Full calculation details are given in *SI Appendix*. We emphasize that, while the in-plane structural tiling in the ideal quasicrystal is aperiodic, it is periodic in the out-of-plane direction. Approximants of quasicrystals are periodic crystals whose local structural motifs match those of the quasicrystal and that, within large unit cells, reproduce a portion of the quasiperiodic structure. $Ta_{21}Te_{13}$ as a platform for calculating the electronic properties of dd-$Ta_{1.6}Te$ and $Ta_{181}Te_{112}$ is a reasonable choice for several reasons: Locally, it has 12-fold symmetric motifs common to both (shown in Fig. 4 *A* and *B*), the local bonding is consistent, and, finally, its unit cell is large enough to capture the relevant physics of the quasicrystalline phase, and the superlarge approximant $Ta_{181}Te_{112}$, yet small enough to be feasible for full ab initio treatment. We note that the use of approximants for the theoretical investigation of quasicrystals has been explored, for example, in twisted graphene bilayers, and their applicability has been proven by direct comparison with full quasicrystal lattices (34, 35). To deduce the layer dependence of the material's electronic structure, we first classified the topological properties of three distinct structures comprising $Ta_{21}Te_{13}$ units: a bulk structure, a monolayer with a 10-Å vacuum, and a bilayer with a 10-Å vacuum. In all cases, they adopt *P6mm* space/layer group

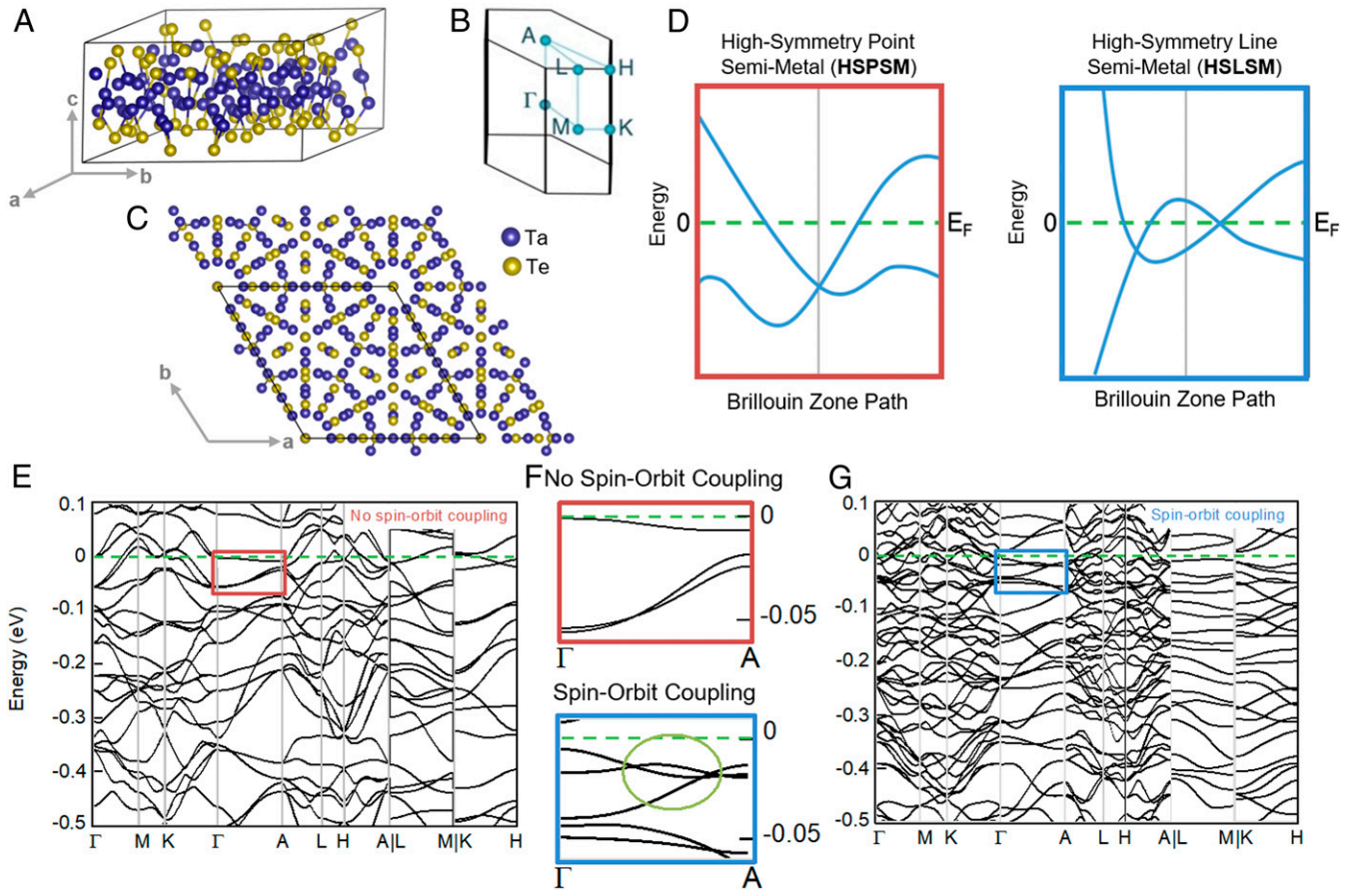

Fig. 4. Electronic structure of the quasicrystal approximant. (*A*) In-plane view, (*B*) Brillouin zone, and (*C*) plane view of the crystalline approximant $Ta_{21}Te_{13}$. (*D*) Schematic of HSPSM and HSLSM band structures. (*E* and *G*) Calculated band structure (*E*) without SOC and (*G*) with SOC of bulk $Ta_{21}Te_{13}$ (HSPSM and HSLSM highlighted by red and blue rectangles, respectively). (*F*) Γ – A section of the band structure showing HSPSM and HSLSM (green oval) within calculated band structure.

symmetry. Topological classification was carried out both with and without spin–orbit coupling (SOC), with the results summarized in Table 1; the Brillouin zone of dd-$Ta_{1.6}Te$ is provided, for reference, in Fig. 4*C*.

First, we discuss the case of bulk $Ta_{21}Te_{13}$: Without SOC, we predict a high-symmetry point semimetal (HSPSM) where the valence and conduction bands meet at the Γ and A high-symmetry points. With SOC, we find a high-symmetry line semimetal (HSLSM) which manifests when the compatibility relations between high-symmetry points in the Brillouin zone are not satisfied; when this occurs, there is at least one topological node along the line connecting the high-symmetry points. Schematics of HSPSM and HSLSM band structures are shown in Fig. 4*D*. In our case, the node occurs on the Γ – A high-symmetry line, which is a two-fold degenerate crossing. To further investigate this, we calculated the electronic band structures of the *P6mm* bulk system with and without SOC, as shown in Fig. 4 *E* and *G*, respectively. Both phases are metallic with several band crossings throughout the Brillouin zone; however, many band degeneracies are lifted with SOC, as expected. We confirm the nodal points at Γ and A in the absence of SOC, and the nodal crossing along the Γ – A line with SOC (Fig. 4*F*). We note that these nodal crossings appear in the out-of-plane direction in the Brillouin zone and so are not protected by quasicrystalline symmetries; however, the out-of-plane structural motifs and hence topological character are common across the quasicrystal and approximant variants.

Table 1. Summary of symmetry-protected topological properties of the $Ta_{21}Te_{13}$ for bulk, bilayer, and monolayer phases

	SOC	Topological classification	Position in Brillouin zone	Bands	Degenerate Irreducible Representation
Bulk	No	HSPSM	A	366 to 367	A_5
			Γ	366 to 367	Γ_5
	Yes	HSLSM	Γ – A line	–	–
Bilayer	No	HSPSM	A	732 to 733	A_5
			Γ	732 to 733	Γ_5
	Yes	Trivial insulator	–	–	–
Monolayer	No	HSLSM	M-Γ, M-A, L-Γ, L-A, M-Γ	–	–
	Yes	Trivial insulator	–	–	–

The topological phases included are HSPSM and HSLSM. For the former, the high-symmetry point coordinates (e.g., M, A, L, Γ) and the corresponding bands are given, while, for the latter, the high-symmetry lines where symmetry-protected crossings appear are listed. Dashes denote Not Applicable.

The bilayer results without SOC are very similar to the bulk case: Our calculations give an HSPSM at Γ and A. However, upon inclusion of SOC, these crossings are gapped out, and the system is reduced to a trivial insulator. We find similar behavior for the properties of the monolayer where, without SOC, we find an HSLSM with nodal crossings throughout the Brillouin zone. These are gapped with the inclusion of SOC, with the monolayer becoming a trivial insulator. From the observation that the bulk and layered compounds have different topological behavior upon the inclusion of SOC, we next examined the topological properties of the bulk compound with changing the magnitude of the interlayer separation in the structure. We find that the bulk structure retains its topological character in varying the nearest interlayer Te–Te separation from its experimental value (1.8 Å) up to 2.8 Å. Beyond this critical point, the bulk structure is topologically trivial. Finally, we calculated the electronic densities of states for the three structures (*SI Appendix*, Fig. S5). All three have almost identical dispersion: Going from bulk to monolayer does not reduce band dispersion.

Next, we discuss the influence of SOC on the symmetry-protected crossings. SOC causes a spin splitting which can be clearly seen in Fig. 4*G*. In the bulk case, this splits the high-symmetry points to a crossing along the high-symmetry line. Moving to the monolayer and bilayer cases, SOC gaps out the nodes, resulting in trivial insulators.

We find that the presence of topological nodal crossings strongly depends on interlayer separation. In our computer experiment, we varied the interlayer separation in the bulk structure, and find a critical value of 2.8 Å, above which the system is a trivial insulator. Physically, modifying the interlayer separation changes the interlayer coupling; in our case, it causes a topological phase transition to occur once the separation is large enough, that is, when exfoliated into few/single layers. This suggests that modifying both the out-of-plane separation, or layer number, and the magnitude of SOC (by chemical substitution with lighter elements) can be used as tuning parameters for controlling the topological phase transitions in these layered materials.

Finally, we address whether our results for the $Ta_{21}Ta_{13}$ periodic approximant are also relevant to the dd phase and $Ta_{181}Te_{112}$. As previously discussed, the main structural changes in going from the approximant to the quasicrystal involved the connectivity of the local structural motifs; however, both phases contain the same local structural ordering, and, importantly, the out-of-plane bonding is the same across structural variants. In addition to the arguments above, that is, similar local structural motifs, and appropriate length scales, we note that the symmetry-projected nodes occur in the out-of-plane Γ − A direction; we confirm that modifications in the interlayer coupling can remove these nodes in the bulk phase. However, the aperiodicity in these systems manifests within the plane, and does not extend into the out-of-plane direction. Therefore, our topological nodal crossings should persist in the quasicrystalline and approximant phases.

In summary, we have isolated a 2D chalcogenide dd quasicrystal and approximant, $Ta_{1.6}Te$. We investigated the structure of the approximant phase with atomic resolution electron microscopy, and explored the topological properties of the materials as a function of layer number. DFT calculations show the presence of a layer-tunable topological band structures, not previously seen in solid-state quasicrystalline systems. Our study lays the groundwork for the study of novel electronic states in low-dimensional quasiperiodic systems, the integration of quasicrystals into van der Waals heterostructures, and the interplay between topology, dimensionality, and symmetry.

Materials and Methods

Samples of the $Ta_{1.6}Te$ were prepared via reduction of $TaTe_2$ with elemental tantalum at high temperatures. Specifically, a 1:3 compressed mixture of $TaTe_2$ and Ta, with iodine as a transport agent, was sealed under argon and heated to 1,700 °C. The 2D samples were prepared within a glove box by mechanical exfoliation using polydimethylsiloxane stamps and identified by optical contrast. A micromanipulator transfer stage was used to transfer 2D samples to SiO_2 substrate and SiN grids. All imaging (TEM and STEM) was conducted at 80 kV to avoid beam damage to the ultrathin samples. Further details of sample preparation and imaging can be found in *SI Appendix*. DFT calculations were performed using the projector augmented wave method in the Vienna ab initio Simulation Package code with the Perdew–Burke–Ernzerhof functionals. Structural parameters for $Ta_{21}Te_{13}$ are extracted from the approximant $Ta_{181}Te_{112}$, and manually fitted to the unit cell of $Ta_{21}Te_{13}$. For the monolayer and bilayer calculation, a vacuum of 10 Å was included in the out-of-plane direction. Topological classification was carried out using DFT calculations and the SymTopo package. Full computational details can be found in *SI Appendix*.

Data Availability. All relevant data can be found herein or in *SI Appendix*.

ACKNOWLEDGMENTS. Support was provided primarily by the US Department of Energy (DOE), Office of Science, Office of Basic Energy Sciences, Materials Sciences and Engineering Division under Contract DE-AC02-05-CH11231, under the sp^2-bonded Materials Program KC2207, which provided for TEM characterization. Additional support was provided by the DOE, Office of Science, Office of Basic Energy Sciences, Materials Sciences and Engineering Division under Contract DE-AC02-05-CH11231, within the van der Waals Heterostructures Program KCWF16, which provided for 2D material preparation and STEM characterization. We also gratefully acknowledge B. Harbrecht and his original work on the material, and W. Hornfeck for his valuable discussion and expertise regarding the material. S.M.G. acknowledges the encouragement and guidance of Alexey Soluyanov throughout this work before his untimely passing. Computational resources were provided by the National Energy Research Scientific Computing Center and the Molecular Foundry, DOE Office of Science User Facilities supported by the Office of Science of the DOE under Contract DE-AC02-05CH11231. The work performed at the Molecular Foundry was supported by the Office of Science, Office of Basic Energy Sciences, of the DOE under the same contract.

1. M. Z. Hasan, C. L. Kane, Colloquium: Topological insulators. *Rev. Mod. Phys.* **82**, 3045–3067 (2010).
2. X. L. Qi, S. C. Zhang, Topological insulators and superconductors. *Rev. Mod. Phys.* **83**, 1057 (2011).
3. F. D. M. Haldane, Model for a quantum Hall effect without Landau levels: Condensed-matter realization of the "parity anomaly.". *Phys. Rev. Lett.* **61**, 2015–2018 (1988).
4. M. A. Silaev, G. E. Volovik, Topological Fermi arcs in superfluid ^{3}He. *Phys. Rev. B Condens. Matter Mater. Phys.* **86**, 214511 (2012).
5. Z. Wang *et al.*, Dirac semimetal and topological phase transitions in A_3Bi (A=Na, K, Rb). *Phys. Rev. B Condens. Matter Mater. Phys.* **85**, 195320 (2012).
6. X. Wan, A. M. Turner, A. Vishwanath, S. Y. Savrasov, Topological semimetal and Fermi-arc surface states in the electronic structure of pyrochlore iridates. *Phys. Rev. B Condens. Matter Mater. Phys.* **83**, 205101 (2011).
7. S. M. Huang *et al.*, A Weyl Fermion semimetal with surface Fermi arcs in the transition metal monopnictide TaAs class. *Nat. Commun.* **6**, 7373 (2015).
8. A. A. Soluyanov *et al.*, Type-II Weyl semimetals. *Nature* **527**, 495–498 (2015).
9. D. Shechtman, I. Blech, D. Gratias, J. W. Cahn, Metallic phase with long-range orientational order and no translational symmetry. *Phys. Rev. Lett.* **53**, 1951–1953 (1984).
10. A. L. Mackay, Crystallography and the Penrose pattern. *Phys. A Stat. Mech. its Appl.* **114**, 609–613 (1982).
11. E. Rotenberg, W. Theis, K. Horn, P. Gille, Quasicrystalline valence bands in decagonal AlNiCo. *Nature* **406**, 602–605 (2000).
12. Y. Nagaoka, H. Zhu, D. Eggert, O. Chen, Single-component quasicrystalline nanocrystal superlattices through flexible polygon tiling rule. *Science* **362**, 1396–1400 (2018).
13. L. Sanchez-Palencia, L. Santos, Bose-Einstein condensates in optical quasicrystal lattices. *Phys. Rev. A* **72**, 053607 (2005).
14. W. Yao *et al.*, Quasicrystalline 30° twisted bilayer graphene as an incommensurate superlattice with strong interlayer coupling. *Proc. Natl. Acad. Sci. U.S.A.* **115**, 6928–6933 (2018).
15. S. Pezzini *et al.*, 30°-twisted bilayer graphene quasicrystals from chemical vapor deposition. *Nano Lett.* **20**, 3313–3319 (2020).
16. S. J. Ahn *et al.*, Dirac electrons in a dodecagonal graphene quasicrystal. *Science* **361**, 782–786 (2018).
17. P. Corbae *et al.*, Evidence for topological surface states in amorphous Bi2Se3. arXiv: 1910.13412v2 (17 February 2020).
18. N. P. Mitchell, L. M. Nash, D. Hexner, A. M. Turner, W. T. M. Irvine, Amorphous topological insulators constructed from random point sets. *Nat. Phys.* **14**, 380–385 (2018).
19. S. A. Mack, S. M. Griffin, J. B. Neaton, Emergence of topological electronic phases in elemental lithium under pressure. *Proc. Natl. Acad. Sci. U.S.A.* **116**, 9197–9201 (2019).

20. H. Huang, F. Liu, Quantum spin Hall effect and spin Bott index in a quasicrystal lattice. *Phys. Rev. Lett.* **121**, 126401 (2018).
21. A. L. He, L. R. Ding, Y. Zhou, Y. F. Wang, C. De Gong, Quasicrystalline Chern insulators. *Phys. Rev. B* **100**, 214109 (2019).
22. D. Varjas *et al*., Topological phases without crystalline counterparts. *Phys. Rev. Lett.* **123**, 196401 (2019).
23. R. Chen, C.-Z. Chen, J.-H. Gao, B. Zhou, D.-H. Xu, Higher-order topological insulators in quasicrystals. *Phys. Rev. Lett.* **124**, 036803 (2020).
24. Y. E. Kraus, Y. Lahini, Z. Ringel, M. Verbin, O. Zilberberg, Topological states and adiabatic pumping in quasicrystals. *Phys. Rev. Lett.* **109**, 106402 (2012).
25. D.-T. Tran, A. Dauphin, N. Goldman, P. Gaspard, Topological Hofstadter insulators in a two-dimensional quasicrystal. *Phys. Rev. B Condens. Matter Mater. Phys.* **91**, 085125 (2015).
26. Y. E. Kraus, Z. Ringel, O. Zilberberg, Four-dimensional quantum Hall effect in a two-dimensional quasicrystal. *Phys. Rev. Lett.* **111**, 226401 (2013).
27. T. Suzuki *et al*., Ultrafast unbalanced electron distributions in quasicrystalline 30° twisted bilayer graphene. *ACS Nano* **13**, 11981–11987 (2019).
28. S. Förster, K. Meinel, R. Hammer, M. Trautmann, W. Widdra, Quasicrystalline structure formation in a classical crystalline thin-film system. *Nature* **502**, 215–218 (2013).
29. M. Conrad, F. Krumeich, B. Harbrecht, A dodecagonal quasicrystalline chalcogenide. *Angew. Chem. Int. Ed. Engl.* **37**, 1383–1386 (1998).
30. M. Conrad, B. Harbrecht, Ta97Te60: A crystalline approximant of a tantalum telluride quasicrystal with twelvefold rotational symmetry. *Chem. Eur. J.* **8**, 3093–3102 (2002).
31. M. Conrad, F. Krumeich, C. Reich, B. Harbrecht, Hexagonal approximants of a dodecagonal tantalum telluride—The crystal structure of $Ta_{21}Te_{13}$. *Mater. Sci. Eng. A* **294–296**, 37–40 (2000).
32. B. E. Brown, The crystal structures of $NbTe_2$ and $TaTe_2$. *Acta Crystallogr.* **20**, 264–267 (1966).
33. P. Stampfli, A dodecagonal quasiperiodic lattice in two dimensions. *Helv. Phys. Acta* **59**, 1260–1263 (1986).
34. G. Yu, Z. Wu, Z. Zhan, M. I. Katsnelson, S. Yuan, Effective band structures of multilayer graphene quasicrystals. arXiv:1908.08439v1 (22 August 2019).
35. G. Yu, Z. Wu, Z. Zhan, M. I. Kastnelson, S. Yuan, Dodecagonal bilayer graphene quasicrystal and its approximants. arXiv:1907.08792v2 (26 July 2019).